化 学 学 报
ACTA CHIMICA SINICA

研究论文
Article

DOI: 10.6023/A12030002

热稳定体相还原态对二氧化钛气敏应用重要性的实验证实

邹晓新[a,b] 李国栋[b] 邹永存[b] 王培培[b] 苏娟[a,b]
赵君[b] 王宇宁[b] 陈接胜*,[a]

([a]上海交通大学化学化工学院 上海 200240)
([b]吉林大学无机合成与制备化学国家重点实验室 长春 130012)

摘要 TiO_2 中体相还原态与气敏性质之间的关系已有理论预测但一直未得到实验验证. 在此, 我们报道一种利用多孔无定型二氧化钛作前驱体制备含热稳定体相还原态 TiO_2 的化学方法. 紫外-可见漫反射光谱, 电子顺磁共振波谱(EPR)以及 X-射线光电子能谱(XPS)证明所获材料中含有的体相还原态为热稳定的 Ti^{3+} 离子以及捕获电子的氧缺位. O_2-程序升温脱附测量结果表明, 体相还原态的存在可以显著提升二氧化钛表面对氧分子的吸附作用. 所获得的体相还原纳米材料不仅表现出优越的对有机分子(乙醇、甲醇及丙酮)的传感性和快速响应性, 而且具有对 CO 传感的良好选择性(相对于 CH_4 和 H_2). 测试结果证实了 TiO_2 传感材料中体相还原态的重要性, 材料的气体传感性能与 TiO_2 表面氧气分子吸附作用密切相关.

关键词 二氧化钛; 气体传感器; 体相还原态; 氧气吸附; 纳米材料

Experimental Validation of the Importance of Thermally Stable Bulk Reduction States in TiO_2 for Gas Sensor Applications

Zou, Xiaoxin[a,b] Li, Guodong[b] Zou, Yongcun[b] Wang, Peipei[b] Su, Juan[a,b]
Zhao, Jun[b] Wang, Yuning[b] Chen, Jiesheng*,[a]

([a] *School of Chemistry and Chemical Engineering, Shanghai Jiao Tong University, Shanghai 200240, China*)
([b] *State Key Laboratory of Inorganic Synthesis and Preparative Chemistry, Jilin University, Changchun 130012, China*)

Abstract The relationship between bulk-reduction states and gas-sensing properties of TiO_2 was predicted previously, but has not been validated yet experimentally. Herein, we present a chemical approach for the preparation of TiO_2 nanoparticles with thermally stable bulk reduction states using porous amorphous titania as precursor. UV/vis diffuse reflectance, electron paramagnetic resonance (EPR) and X-ray photoelectron spectroscopy (XPS) confirm that the stable bulk reduction states are the thermally stable Ti^{3+} ions and electron-trapped oxygen vacancies. O_2-temperature programmed desorption (O_2-TPD) measurements demonstrate that the presence of the bulk reduction states can obviously enhance the oxygen adsorption on titania surfaces. Furthermore, the bulk-reduced nanomaterial exhibits not only enhanced sensitivity and ultrafast response/recovery (＜3 s) for the detection of organic vapors (ethanol, methanol and acetone), but also excellent selectivity to CO against CH_4 and H_2. The sensing performance testing results confirm the importance of bulk reduction states in TiO_2 sensors for the first time, and the enhanced gas-sensing performances for bulk-reduced TiO_2 materials can be related to the enhanced oxygen absorption on TiO_2 surfaces.

Keywords titanium dioxide; gas sensor; bulk reduction states; oxygen adsorption; nanomaterial

1 Introduction

Titanium dioxide (TiO_2) is one of the most important oxide semiconductors. Enormous efforts have been devoted to the research of TiO_2 materials in the past decades, and many promising applications such as photocatalysis, photovoltaics, and sensing have been successfully developed.[1] These applications depend not only on the intrinsic properties of TiO_2 but also strongly on its microstructure which affects the functions of TiO_2 to a great extent.[2] Therefore, it is of great significance to establish the relationship between microstructure and function of TiO_2 material, and to enhance its performance through microstructure-tuning.

Reduced TiO_2 is a unique titania material with a non-stoichiometric composition, and a large number of reduction states (Ti^{3+} ions and oxygen vacancies) are present in the material.[3-13] The presence of reduction states has been theoretically and/or experimentally confirmed to play an important role in modifying energy band and surface

* E-mail: chemcj@sjtu.edu.cn
Received February 28, 2012; published March 30, 2012.
Supporting information for this article is available free of charge via the Internet at http://sioc-journal.cn
Project supported by the National Natural Science Foundation of China (91022019) and the National Basic Research Program of China (2011CB808703).
项目受国家自然科学基金(No. 91022019)和国家重点基础研究计划(No. 2011CB808703)资助.

structures of TiO_2,[9,13] and in varying its magnetic,[7,8] electronic[11] and photocatalytic behavior.[11-13] Gas-sensing is a typical property of metal oxide semiconductor materials such as titania, and this property is associated with conductivity variation, which is induced by the interaction between the adsorbed oxygen on the surface of the semiconductor and the gas molecules to be detected.[14] Recently, surface chemistry studies revealed that the bulk reduction states control the oxygen adsorption chemistry on titania surfaces.[15] Considering the strong correlation between oxygen adsorption on oxide semiconductor surface and gas-sensing performance, it was predicted that the bulk reduction states would have a strong influence on the gas-sensing properties of TiO_2 materials,[15] but yet no experimental evidence is available to support this convincingly.

Herein, we report the preparation of TiO_2 nanoparticles with a mass of thermally stable bulk reduction states using porous amorphous titania as precursor. The bulk-reduced nanomaterial shows not only substantially enhanced sensitivity and ultrafast response/recovery for the detection of organic vapors, but also excellent selectivity to CO against CH_4 and H_2, demonstrating the importance of bulk reduction states in TiO_2 sensor. The bulk "self-doping" approach to enhance gas-sensing performance of semiconductor oxides is unique because previously surface-doping with metals and/or oxides was widely described in the literature to overcome the inherent shortcomings of pure oxide sensing materials.[14] In addition, the "self-doping" strategy is simple and cost-effective, avoiding the complexity of multi-component system and/or the high cost of noble metals.

2 Results and discussion

Two bulk-reduced TiO_2 samples were prepared through calcining a porous amorphous titania in air in the presence of imidazole and hydrochloric acid at 500 and 600 ℃ for 2 h, respectively (Figure 1). The corresponding TiO_2 samples are denoted as TiO_2-500 and TiO_2-600, respectively. In contrast, no bulk-reduced TiO_2 samples can be obtained when either imidazole or hydrochloric acid was not added in the above reaction system, or nitric acid/acetic acide with the same concentration was used to replace hydrochloric acid. These results indicate that the combustion of imidazole in the presence of hydrochloric acid is indispensable to the generation of reducing gases and thus the formation of the bulk-reduced TiO_2. In addition, the porous amorphous titania precursor was obtained through UV-light irradiation of titanium glycolate.[7] SEM, N_2 adsorption and X-ray diffraction measurements (Figure 2) demonstrate that the porous titania precursor was an amorphous material with a BET surface area of 530 m^2/g and a particle size of >1 μm. For comparison, non-porous TiO_2 samples with anatase or rutile structures have been used as precursors to replace the porous amorphous TiO_2, but no bulk-reduced TiO_2 materials are obtained under identical reaction conditions. The uniqueness of the porous TiO_2 precursor may lie in its porous structure with a high surface area. The porous feature renders it easy for the TiO_2 precursor to interact with the reducing gases, which are *in situ* produced via combustion of imidazole.

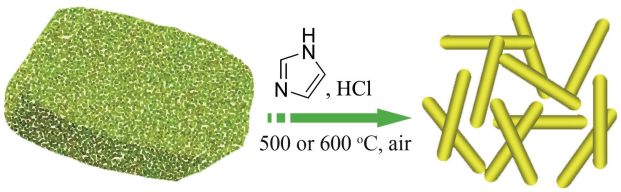

Figure 1 Schematic representation for the formation of the bulk-reduced TiO_2 material from porous amorphous titania precursor.

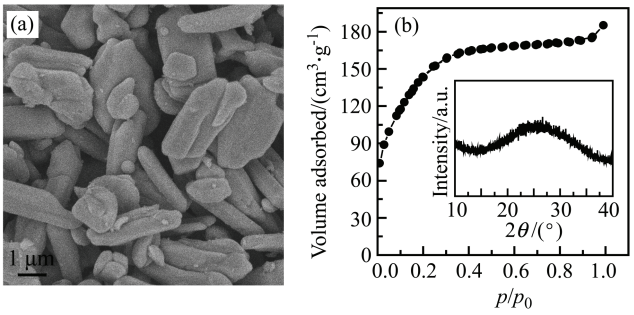

Figure 2 (a) SEM image, (b) N_2 adsorption/desorption isotherms of the porous amorphous titania precursor. Its XRD pattern is shown in the inset of Figure 2b.

The SEM images (Figure 3) show that the two bulk-reduced TiO_2 materials are mainly composed of rod-like nanoparticles with a width of 20—30 nm and a length up to 100—300 nm. Obviously, the particle size of two bulk-reduced TiO_2 materials is far smaller than the porous amorphous titania precursor (Figure 2a), indicating that the *in situ* produced reducing gases crack the particle of the original porous titania precursor, and a process of recrystallization and growth of crystalline TiO_2 nanparticles occurs. This is confirmed by the fact that when no reducing gases are involved in the reaction system, the morphology of the porous titania precursor varies only slightly. The X-ray diffraction (XRD) characterization (Figure 4) shows that TiO_2-500 is dominated by rutile with a tiny amount of anatase, whereas TiO_2-600 is identified as pure rutile.

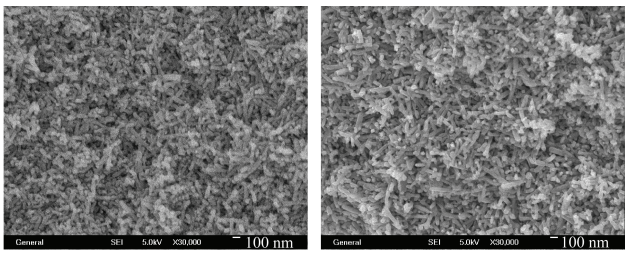

Figure 3 SEM images of TiO_2-500 (left) and TiO_2-600 (right).

Figure 5a presents the UV/vis diffuse reflectance spectra for the two bulk-reduced samples and a rutile TiO_2 reference material without bulk reduction states (hereafter denoted as R-TiO_2). The R-TiO_2 sample exhibits an inherent bandgap absorption in the ultraviolet region with a threshold of about 410 nm. Differing from the R-TiO_2 sample, the two bulk-reduced TiO_2 samples show not only a strong

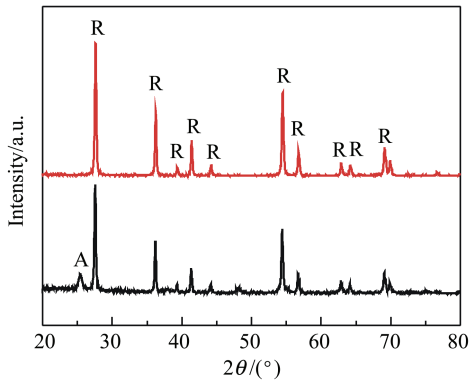

Figure 4 XRD patterns of TiO_2-500 (down) and TiO_2-600 (up). A and R denote anatase and rutile, respectively.

UV absorption similar to that of R-TiO_2, but also an obvious visible-light absorption covering the whole visible-light region. This type of visible-light absorption is related to the reduction states in TiO_2 (*e.g.*, single-electron-trapped oxygen vacancies ($V_o^{\bullet}$) and Ti^{3+} species).[3-13,16] The stronger visible-light absorption for TiO_2-500 indicates the larger amount of reduction states in TiO_2-500. The optical properties are in agreement with the colors (Figure 5b) of TiO_2-500 (dark gray), TiO_2-600 (light gray) and R-TiO_2 (white).

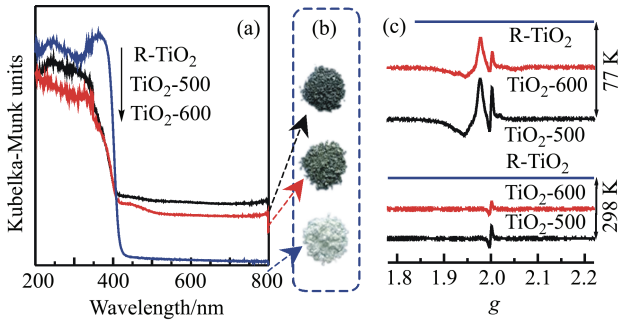

Figure 5 (a) UV/vis diffuse reflectance spectra, (b) photos, and (c) EPR spectra measured at 298 K and 77 K of TiO_2-500 (black line) and TiO_2-600 (red line). For comparison, the UV/vis diffuse reflectance spectrum, photo and EPR spectra of R-TiO_2 are also provided (blue line).

Because the $V_o^{\bullet}$ and Ti^{3+} species are paramagnetic, the electron paramagnetic resonance (EPR) spectra (Figure 5c) of the two bulk-reduced TiO_2 samples were recorded at both room temperature (298 K) and 77 K. The TiO_2-500 and TiO_2-600 samples show a distinct singlet signal at g= 2.002 at 298 K, and this EPR signal is ascribed to the $V_o^{\bullet}$ species.[11,16] When the measurement temperature decreases to 77 K, the signal intensity at g=2.002 increases, suggesting that the relaxation time of the trapped electrons becomes longer. More importantly, a new, asymmetrical EPR signal at g<2.000, which is assignable to Ti^{3+} ($3d^1$) ions in TiO_2 lattice,[5,17] shows up. The higher EPR signal intensity of TiO_2-500 in comparison with that of TiO_2-600 indicates that more reduction states (Ti^{3+} and $V_o^{\bullet}$) are present in TiO_2-500. Furthermore, the EPR data also indicate that these reduction states are present in the bulk, rather than on the surface of the TiO_2 nanparticles because the reduction states would be easily oxidized by O_2 in air if they were on the surface of the TiO_2 sample. The Ti2p XPS spectra (Figure 6) for the two bulk-reduced samples further confirm that the surface of the two samples is dominated by Ti^{4+}, without presence of Ti^{3+} species. The perfect combination of the bulk-reduced feature and the excellent thermal stability in one material is important for exploration of gas-sensing performances of the bulk-reduced TiO_2 materials (The two bulk-reduced samples are thermally stable up to 500 ℃ in air without disappearance of bulk reduction states and crystal structure variation).

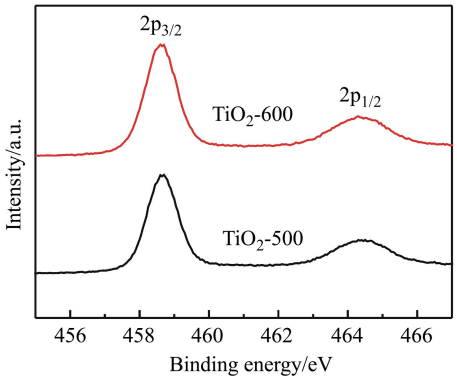

Figure 6 XPS spectra of Ti2p for TiO_2-500 (black line), and TiO_2-600 (red line).

A typical sensor was fabricated conveniently by pasting viscous slurry of the bulk-reduced TiO_2 material onto an alumina tube with a diameter of 1 mm and a length of 4 mm, which was positioned with a pair of Au electrodes and four Pt wires on both ends of the tube (Figure 7). A Ni-Cr alloy coil through the tube was employed as a heater to control the operating temperature. The optimal operating temperature for the sensor was 300 ℃. The sensor sensitivity is defined as the ratio R_a/R_g, where R_a and R_g are the electrical resistance of the sensor in atmospheric air and in the testing gas, respectively. The response and recovery times are defined as the times taken by the sensor to achieve 90% of the total resistance change in the case of adsorption and desorption, respectively.

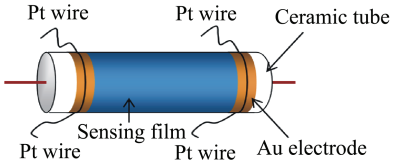

Figure 7 Schematic diagram showing the structure of a typical gas sensor.

The sensing performance of TiO_2-500 was evaluated using ethanol as the testing gas. Figure 8a shows the dynamic response-recovery curve of the TiO_2-500 sensor with increasing ethanol concentrations. It is seen that the sensor has a wide response range for ethanol from 5 to 500 ppm. When exposed to 5 ppm ethanol, the sensitivity of the sensor is about 2.6. The sensitivity increases significantly with increasing ethanol concentration. For ethanol concentrations of 10, 20, 50, 100, 200, and 500 ppm, the sensitivities are about 3.5, 5.4, 7.3, 11.5, 19.0, and 41.3, respectively. For comparison, the sensing

performances of TiO_2-600 and R-TiO_2 have also been tested, and it is demonstrated (Figure 8b) that the sensitivity values are in such an order as TiO_2-500＞TiO_2-600＞R-TiO_2. The sensitivity of TiO_2-500 is about 5.4 times as high as that of R-TiO_2 in the presence of 500 ppm ethanol. The stability of the TiO_2-500 sensor is also very high because the sensitivity of this sensor is not decreased even after exposure in 50 ppm ethanol for 30 days. Furthermore, methanol and acetone were also used as the testing gases, and a distinctly enhanced sensitivity was observed as well for the bulk-reduced samples (Figures 8c — 8f) in comparison with the R-TiO_2 material.

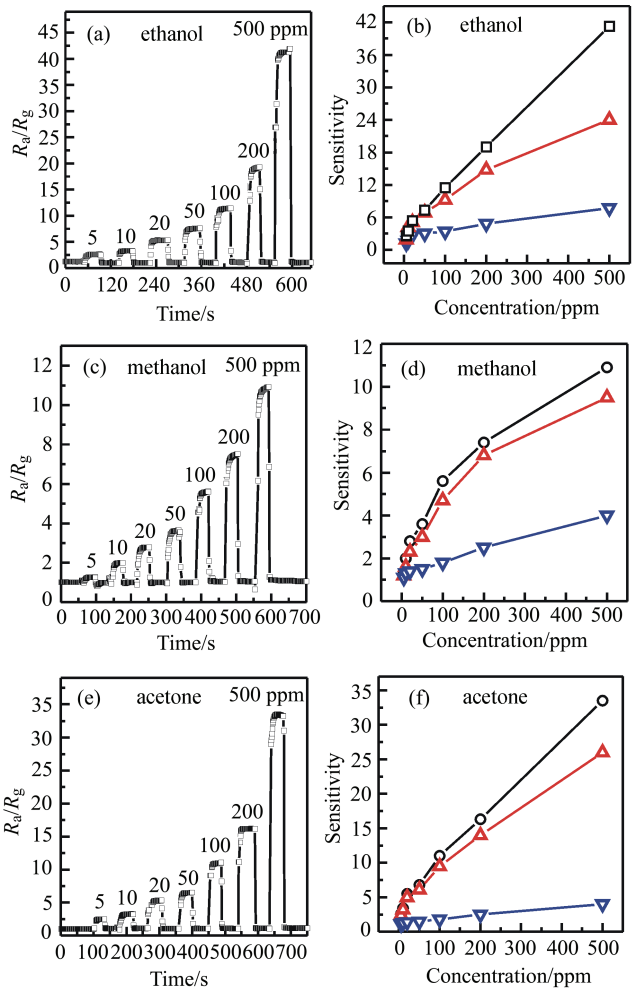

Figure 8 Dynamic response-recovery curves of the sensor based on TiO_2-500 for (a) ethanol, (c) methanol and (e) acetone detection; and the corresponding comparisons of the gas concentration-dependent sensitivities of TiO_2-500 (○), TiO_2-600 (△) and R-TiO_2 (▽).

In addition to sensitivity, response and recovery times are also critical for a gas sensor. From Figures 8a, 8c, and 8e, it is seen that the response and recovery of the TiO_2-500 sensor are ultrafast for the detection of organic vapors (ethanol, methanol and acetone), and the times of response and recovery are less than 3 s. Such fast response and recovery were not observed in previous TiO_2-based sensors for the detection of organic vapors (in general the recovery time was longer than 30 s).[18] Furthermore, in comparison with other common oxide sensing materials (*e.g.*, ZnO, WO_3, and In_2O_3),[19] the TiO_2-500 material is also advantageous because fast recovery (＜10 s) is usually difficult to achieve for those oxide materials. The above results demonstrate that the bulk-reduced TiO_2 material (TiO_2-500) are rather promising for use in fast and continuous detection/monitoring of organic vapors.

The sensor based on TiO_2-500 was also found to exhibit excellent selectivity for the detection of CO against CH_4 and H_2. Continuous CO monitoring for incomplete combustion of gas appliances is very important to prevent CO poisoning accidents, and the sensor for this purpose must have high CO selectivity against co-existing gases such as H_2, and CH_4.[20] As shown in Figure 9, TiO_2-500 responds to CO gas with a nearly linear sensitivity variation from 100 to 10000 ppm, whereas it does not respond to CH_4 and H_2 at all. In contrast, R-TiO_2 shows no response to all these gases.

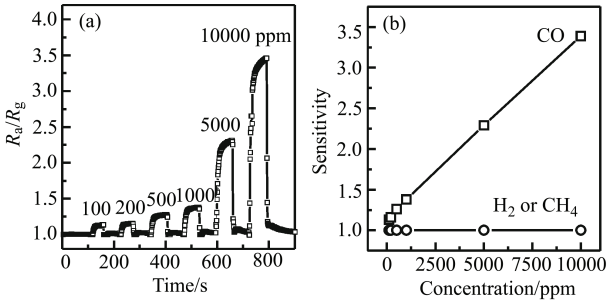

Figure 9 (a) Dynamic response-recovery curve of the sensor based on TiO_2-500 for the CO detection; (b) the corresponding concentration-dependent sensitivities for the detection of CO, CH_4 and H_2.

To further confirm the importance of bulk reduction states in TiO_2 sensor, the possible influencing factors such as crystal phase and surface area are excluded. Considering that TiO_2-500 contains anatase and rutile, the gas-sensing performance of anatase TiO_2 was also tested (Figure S1 in Supporting Information). Anatase TiO_2 exhibits very similar gas sensing properties to R-TiO_2 (very low response to ethanol, methanol, and acetone vapors), demonstrating that crystal phase is not important in determining the gas sensing properties of TiO_2. In addition, TiO_2-500, TiO_2-600 and R-TiO_2 possess similar surface areas (＜10 m^2/g), and thus surface area is also not the reason behind the enhanced sensing performance of TiO_2-500.

As reported previously, the bulk reduction states can control the oxygen adsorption chemistry on titania surfaces.[15] Similar behavior (Figure 10) has also been observed in our work for the titania materials. The amount of chemisorbed oxygen was obtained by O_2-temperature programmed desorption (O_2-TPD) to be 4.56, 2.18 and 0.76 mmol/g for TiO_2-500, TiO_2-600 and R-TiO_2, respectively. Obviously, the bulk-reduced samples chemisorb much more oxygen than R-TiO_2.

The gas sensing behavior for a metal oxide semiconductor is generally ascribed to the interaction of surface chemisorbed oxygen and the gas molecules to be detected. Figure 11 shows the schematic representation of sensing mechanism of bulk-reduced TiO_2. When a titania sensor is

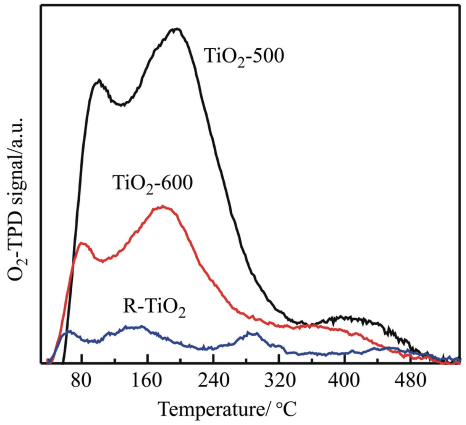

Figure 10 TPD-O_2 curves of TiO_2-500, TiO_2-600 and R-TiO_2.

operated at a moderate temperature in air, the oxygen in the atmosphere are adsorbed on the surface of titania with negative charges. The extraction of electrons by oxygen from the crystal surface generates an electron depletion layer, leading to formation of a potential barrier near the grain boundary and a corresponding high resistance state. When the sensor is exposed to a reductive gas such as ethanol and CO, the gas reacts with the adsorbed oxygen, resulting in a decrease of the amount of adsorbed oxygen. As a consequence, the height of the potential barrier is reduced, and the resistance of the whole sensing layer decreases to a great extent. Evidently, the key step in sensing process is the interaction between surface chemisorbed oxygen and the gas molecules to be detected. The increase in amount of surface adsorbed oxygen enhances this interaction, promoting the performance of the gas sensor.[21] The bulk-reduced titania material we obtained can chemisorb a large amount of oxygen, and therefore its sensing performance is greatly enhanced in comparison with those without bulk-reduced states.

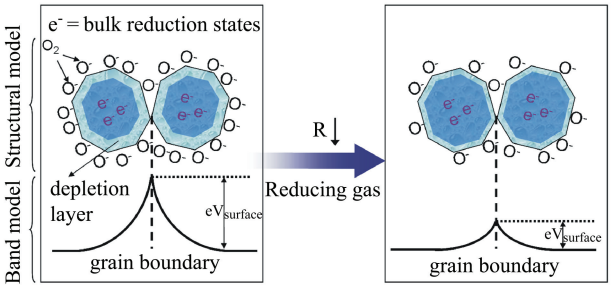

Figure 11 Schematic representation of sensing mechanism of the bulk-reduced TiO_2. e^- and O^- denote the bulk reduction states and surface adsorbed oxygen.

3 Conclusion

In summary, using a porous amorphous titania as precursor, we have successfully prepared bulk-reduced TiO_2 nanoparticles with a satisfactory thermal stability and superior gas-sensing properties. Our experimental observations validate that the presence of bulk reduction states in TiO_2 indeed play an important role in enhancing gas-sensing performances. The results presented herein sets forth a new avenue to rationally design and develop new types of high-performance nanosized materials by bulk-microstructure tuning.

4 Experimental section

4.1 Preparation of porous amorphous titania precursor

The porous amorphous titania precursor was prepared through a light-driven approach.[7] Typically, titanium glycolate (4.0 g), which was synthesized on a large scale according to the reported procedure,[22] was dispersed in water (300 mL) and then exposed to UV-light irradiation for 1 h. After the irradiation, the color of the solid sample turned from white (titanium glycolate) to intense blue because of the presence of Ti^{3+}.[7] Finally, the blue solid product was separated from the mixture and dried in air, the O_2 molecules of which oxidize the Ti^{3+} to Ti^{4+} because the Ti^{3+} species are on the surface (internal and external) of the solid. The obtained product was the porous amorphous titania precursor described in this paper. The amorphous and porous feature of this precursor material was confirmed by X-ray diffraction and adsorption measurements. The BET surface area of the porous TiO_2 precursor was about 530 m^2/g. The UV-light source used in the experiment was a 125 W high-pressure mercury lamp, and the irradiation intensity of the UV-light was about 9.0×10^4 μW/cm^2.

4.2 Preparation of bulk-reduced TiO_2 nanopowder samples

Two bulk-reduced TiO_2 samples were easily prepared via heating the mixture of the porous TiO_2 precursor (0.5 g), imidazole (2 g) and hydrochloric acid (HCl, 37 wt%, 3 mL) in a muffle furnace at 500 and 600 ℃ for 2 h, respectively. After cooling to room temperature, the final products were collected, and the corresponding TiO_2 samples are designated as TiO_2-500 and TiO_2-600, respectively. The colors of TiO_2-500 and TiO_2-600 are dark gray and light gray, respectively.

4.3 Control experiments

Rutile TiO_2 (R-TiO_2) was prepared by directly calcining the porous amorphous titania precursor in a muffle furnace at 700 ℃ for 2 h. Anatase TiO_2 was prepared by directly calcining the porous amorphous titania precursor in a muffle furnace at 500 ℃ for 2 h.

4.4 General characterization

The powder X-ray diffraction (XRD) patterns were recorded on a Rigaku D/Max 2550 X-ray diffractometer with Cu Kα radiation (λ=1.5418 Å) operated at 200 mA and 40 kV. The scanning electron microscopic (SEM) images were taken on a JEOL JSM 6700F electron microscope. The UV/vis diffuse reflectance spectra were recorded on a Perkin-Elmer Lambda 20 UV/Vis spectrometer. The electron paramagnetic resonance (EPR) spectra were recorded on a JEOL JES-FA 200 EPR spectrometer. The X-ray photoelectron spectroscopy (XPS) was performed on an ESCALAB 250 X-ray photoelectron spectrometer with a monochromated X-ray source (Al Kα $h\upsilon$=1486.6 eV). The energy scale of the spectrometer was calibrated using $Au4f_{7/2}$, $Cu2p_{3/2}$, and $Ag3d_{5/2}$ peak positions. The standard deviation for the binding energy (BE) values was 0.1 eV.

The O_2-temperature programmed desorption (O_2-TPD) was performed using an Automated Catalyst Characterization System (AutoChem II 2920 V3.05, Micromeritics Instrument Corporation). For a typical TPD experiment, 100 mg of sample was pretreated under a flow of 10% O_2 in Ar (20 mL/min) at 300 ℃ for 2 h and then cooled down to 50 ℃ under the same flow. The sample was then swept by a He flow of 30 mL/min for 2 h. The TPD-O_2 was performed with a temperature ramp of 5 ℃/min from 50 to 500 ℃ under a He flow of 10 mL/min. Oxygen was monitored and quantified using a thermal conductivity detector.

4.5 Sensor fabrication and performance testing

The gas sensor was fabricated by pasting viscous slurry of the bulk-reduced TiO_2 sample onto an alumina tube with a diameter of 1 mm and a length of 4 mm, which was positioned with a pair of Au electrodes and four Pt wires on both ends of the tube.[23] A Ni-Cr alloy coil through the tube was employed as a heater to control the operating temperature. Gas sensing tests were performed on a commercial CGS-8 Gas Sensing Measurement System (Beijing Elite Tech Company Limited). The sensor sensitivity is defined as the ratio R_a/R_g, where R_a and R_g are the electrical resistance of the sensor in atmospheric air and in the testing gas, respectively. The response and recovery times are defined as the times taken by the sensor to achieve 90% of the total resistance change in the case of adsorption and desorption, respectively.

References

[1] Chen, X.; Mao, S. S. *Chem. Rev.* **2007**, *107*, 2891.

[2] (a) Wu, N.; Wang, J.; Tafen, D. N.; Wang, H.; Zheng, J.; Lewis, J. P.; Liu, X.; Leonard, S. S.; Manivannan, A. *J. Am. Chem. Soc.* **2010**, *132*, 6679; (b) Kang, S. H.; Choi, S.; Kang, M.; Kim, J.; Kim, H.; Hyeon, T.; Sung, Y. *Adv. Mater.* **2008**, *20*, 54; (c) Zou, X.-X.; Li, G.-D.; Wang, Y.-N.; Zhao, J.; Yan, C.; Guo, M.-Y.; Li, L.; Chen, J.-S. *Chem. Commun.* **2011**, *47*, 1066; (d) Chen, X.; Liu, L.; Yu, P. Y.; Mao, S. S. *Science* **2011**, *331*, 746.

[3] Valentin, C. D.; Pacchioni, G.; Selloni, A. *J. Phys. Chem. C* **2009**, *113*, 20543.

[4] Livraghi, S.; Maurelli, S.; Paganini, M. C.; Chiesa, M.; Giamello, E. *Angew. Chem. Int. Ed.* **2011**, *123*, 8188.

[5] Khomenko, V. M.; Langer, K.; Rager, H.; Fett, A. *Phys. Chem. Miner.* **1998**, *25*, 338.

[6] He, Y.; Dulub, O.; Cheng, Y.; Selloni, A.; Diebold, U. *Phys. Rev. Lett.* **2009**, *102*, 106105.

[7] Zou, X.-X.; Li, G.-D.; Wang, K.-X.; Li, L.; Su, J.; Chen, J.-S. *Chem. Commun.* **2010**, *46*, 2112.

[8] Zhao, Q.; Wu, P.; Li, B. L.; Lu, Z. M.; Jiang, E. Y. *J. Appl. Phys.* **2008**, *104*, 073911.

[9] Li, M.; Hebenstreit, W.; Diebold, U.; Tyryshkin, A. M.; Bowman, M. K.; Dunham, G. G.; Henderson, M. A. *J. Phys. Chem. B* **2000**, *104*, 4944.

[10] Yagi, E.; Hasiguti, R. R.; Aono, M. *Phys. Rev. B* **1996**, *54*, 7945.

[11] Nakamura, I.; Negishi, N.; Kutsuna, S.; Ihara, T.; Sugihara, S. Takeuchi, K. *J. Mol. Catal. A* **2000**, *161*, 205.

[12] Liu, G.; Yang, H. G.; Wang, X.; Cheng, L.; Lu, H.; Wang, L.; Lu, G. Q.; Cheng, H.-M. *J. Phys. Chem. C* **2009**, *113*, 21784.

[13] Zuo, F.; Wang, L.; Wu, T.; Zhang, Z.; Borchardt, D.; Feng, P. *J. Am. Chem. Soc.* **2010**, *132*, 11856.

[14] Franke, M. E.; Koplin, T. G.; Simon, U. *Small* **2006**, *2*, 36.

[15] Lira, E.; Wendt, S.; Huo, P.; Hansen, J. Ø.; Streber, R.; Porsgaard, S.; Wei, Y.; Bechstein, R.; Lægsgaard, E.; Besenbacher, F. *J. Am. Chem. Soc.* **2011**, *133*, 6529.

[16] Qian, L.; Jin, Z. S.; Zhang, J. W.; Huang, Y. B.; Zhang, Z. J.; Du, Z. L. *Appl. Phys. A* **2005**, *80*, 1801.

[17] Dimitrijevic, N. M.; Saponjic, Z. V.; Rabatic, B. M.; Poluektov, O. G.; Rajh, T. *J. Phys. Chem. C* **2007**, *111*, 14597.

[18] (a) Garzella, C.; Comini, E.; Tempesti, E.; Frigeri, C.; Sberveglieri, G. *Sens. Actuators B* **2000**, *68*, 189; (b) Garzella, C.; Bontempi, E.; Depero, L. E.; Vomiero, A.; Mea, G. D.; Sberveglieri, G. *Sens. Actuators B* **2003**, *93*, 495; (c) Benkstein, K. D.; Semancik, S. *Sens. Actuators B* **2006**, *113*, 445.

[19] (a) Jing, Z.; Zhan, J. *Adv. Mater.* **2008**, *20*, 4547; (b) Chen, D.; Hou, X.; Wen, H.; Wang, Y.; Wang, H.; Li, X.; Zhang, R.; Lu, H.; Xu, H.; Guan, S.; Sun, J.; Gao, L. *Nanotechnology* **2010**, *21*, 035501; (c) Kim, S.-J.; Hwang, I.-S.; Na, C. W.; Kim, I.-D.; Kang, Y. C.; Lee, J.-H. *J. Mater. Chem.* **2011**, *21*, 18560.

[20] (a) Yamaura, H.; Tamaki, J.; Moriya, K.; Miura, N.; Yamazoe, N. *J. Electrochem. Soc.* **1997**, *144*, L158; (b) Yamaura, H.; Jinkawa, T.; Tamaki, J.; Moriya, K.; Miura, N.; Yamazoe, N. *Sens. Actuators B* **1996**, *35-36*, 325; (c) Sedghi, S. M.; Mortazavi, Y.; Khodadadi, A. *Sens. Actuators B* **2010**, *145*, 7; (d) Yu, J. H.; Choi, G. M. *Sens. Actuators B* **2001**, *75*, 56; (e) Moon, W. J.; Yu, J. H.; Choi, G. M. *Sens. Actuators B* **2001**, *80*, 21.

[21] (a) Kocemba, I.; Rynkowski, J. *Sens. Actuators B* **2011**, *155*, 659; (b) Saukko, S.; Lassi, U.; Lantto, V.; Kroneld, M.; Novikov, S.; Kuivalainen, P.; Rantala, T. T.; Mizsei, J. *Thin Solid Films* **2005**, *490*, 48.

[22] Zou, X.-X.; Li, G.-D.; Guo, M.-Y.; Li, X.-H.; Liu, D.-P.; Su, J.; Chen, J.-S. *Chem.-Eur. J.* **2008**, *14*, 11123.

[23] Zou, X.-X.; Li, G.-D.; Zhao, J.; Wang, P.-P.; Wang, Y.-N.; Zhou, L.-J.; Su, J.; Li, L.; Chen, J.-S. *Inorg. Chem.* **2011**, *50*, 9106.

(Cheng, B.)

